Ocean Sci. Discuss., 10, 1647–1705, 2013
www.ocean-sci-discuss.net/10/1647/2013/
doi:10.5194/osd-10-1647-2013

Ocean Science
Discussions
Open Access

Ventilation of the Mediterranean Sea constrained by multiple transient tracer measurements

T. Stöven and T. Tanhua

GEOMAR Helmholtz Centre for Ocean Research Kiel, Kiel, Germany

Received: 9 September 2013 – Accepted: 21 September 2013 – Published: 10 October 2013

Correspondence to: T. Stöven (tstoeven@geomar.de)

Published by Copernicus Publications on behalf of the European Geosciences Union.

Abstract

Ventilation is the prime pathway for ocean surface perturbations, such as temperature anomalies, to be relayed to the ocean interior. It is also the conduit for gas exchange between atmosphere and ocean and thus the mechanism whereby, for instance, the interior ocean is oxygenated and enriched in anthropogenic carbon. The ventilation of the Mediterranean Sea is fast in comparison to the world ocean and has large temporal variability, so that quantification of Mediterranean Sea ventilation rates is challenging and very relevant for Mediterranean oceanography and biogeochemistry. Here we present transient tracer data from a field-campaign in April 2011 that sampled a unique suite of transient tracers (SF_6, CFC-12, tritium and ^3He) in all major basins of the Mediterranean. We apply the Transit Time Distribution (TTD) model to the data which then constrain the mean age, the ratio of the advective/diffusive transport mechanism, and the presence, or not, of more than one significant (for ventilation) water mass.

We find that the eastern part of the Eastern Mediterranean can be reasonable described with a one dimensional Inverse Gaussian (1IG) TTD, and thus constrained with two independent tracers. The ventilation of the Ionian Sea and the Western Mediterranean can only be constrained by a multidimensional TTD. We approximate the ventilation with a two-dimensional Inverse Gaussian (2IG) TTD for these areas and demonstrate one way of constraining a 2IG-TTD from the available transient tracer data. The deep water in the Ionian Sea has higher mean ages than the deep water of the Levantine Basin despite higher transient tracer concentrations. This is partly due to the deep water of Adriatic origin having more diffusive properties in the transport and formation, i.e. a high ratio of diffusion over advection, compared to the deep water of Aegean Sea origin that still dominates the deep Levantine Basin deep water after the Eastern Mediterranean Transient (EMT) in the early 1990s. We also show that the deep Western Mediterranean has approximately 40% contribution of recently ventilated deep water from the Western Mediterranean Transition (WMT) event of the mid-2000s. The

OSD
10, 1647–1705, 2013

deep water has higher transient tracer concentrations than the mid-depth water, but the mean age is similar.

1 Introduction

The Mediterranean Sea is a marginal sea, where the observational record shows distinctive variability and trends. The most prominent transient event in the Eastern Mediterranean Sea (EMed) is the transfer of the deep water source from the Adriatic Sea to the Aegean and Cretan Sea and vice versa. The observed massive dense water input from the Aegean and Cretan Sea in the early 1990s is known as the Eastern Mediterranean Transient (EMT) (Roether et al., 1996; Klein et al., 1999; Lascaratos et al., 1999). The extensive deep water formation in the Western Mediterranean Sea (WMed) between 2004–2006, known as the Western Mediterranean Transition (WMT) (Schroeder et al., 2008, 2010), is presumed to be triggered respectively preconditioned by the EMT event (Schroeder et al., 2006). Nevertheless, both events are part of a general circulation pattern which can be observed in the Mediterranean Sea. The surface water in the Western Mediterranean Sea (WMed) is supplied by less dense Atlantic Water (AW) through the Strait of Gibraltar. The AW flows eastwards at shallow depth < 200 m into the Tyrrhenian Sea and into the EMed via the Strait of Sicily. The salinity of the AW increases along the pathway from 36.5 to > 38 due to net evaporation and is then described as Modified Atlantic Water (MAW) (Wuest, 1961). The heat loss during winter time of the MAW in the EMed leads to a sufficient increase of density to form the Levantine Intermediate Water (LIW) at depth between 200–600 m (Brasseur et al., 1996; Wuest, 1961). The exact area of the LIW formation process is uncertain and possibly variable, but it is expected to be in the eastern part of the EMed near Rhodes (Malanotte-Rizzoli and Hecht, 1988; Lascaratos et al., 1993; Roether et al., 1998). The main volume of the LIW flows back westwards over the shallow sill between Sicily and Tunisia entering the Tyrrhenian Sea along the continental slope of Italy (Wuest, 1961). Parts of the LIW enter the Adriatic Sea via the Strait of Otranto,

OSD
10, 1647–1705, 2013

where it serves as an initial source of the Adriatic Sea Overflow Water (ASOW). The formation of ASOW in the Adriatic Pit is based on interactions between the LIW and water masses coming from the northern Adriatic Sea as well as the natural preconditioning factors, e.g. wind stress and heat loss (Artegiani et al., 1996a, b). The ASOW flows over the sill of Otranto into the Ionian Sea intruding the bottom layer and thus representing a source of the Eastern Mediterranean Deep Water (EMDW) (Schlitzer et al., 1991; Roether and Schlitzer, 1991). Furthermore, the Ionian Sea is connected with the Levantine Sea via the Cretan Passage, following that parts of newly formed EMDW also reach the deep water of the Levantine Sea. In 1992/93 the water mass conditions in the well ventilated Aegean and Cretan Sea changed into a more salty and cold state, sufficient enough to initialize the massive dense water input of Cretan Deep Water (CDW) into the abyssal basins of the EMed (Klein et al., 1999). This EMT event led to a disruption of the usual formation pattern of the EMDW. The Adriaitc Sea as major deep water source was thereby replaced by the Aegean and Cretan Sea with the consequence that the bottom layer of the Ionian Sea was now supplied with dense water via the Antikythera Strait and the Levantine Sea via the Kasos Strait. Not only the simultaneous dense water input into both basins, but also the large amount of the outflow caused an uplift of the intermediate water layers in the Ionian and Levantine Sea. One consequence of the EMT seems to be the preconditioning of the WMT in 2004–2006 by uplifted water masses entering the WMed via the Strait of Sicily. An extensive deep water formation in the WMed took place in the Gulf of Lyon and the Balearic Sea, whereat the major triggering factor was the heat loss due to the Mistral in this area. Although the total magnitude of the WMT was smaller than the one of the EMT it effects nearly a complete renewal of the Western Mediterranean Deep Water (WMDW). Recent water mass analyses indicate, that the EMed is returning to a pre EMT state with the Adriatic Sea as major deep water source (Hainbucher et al., 2006; Rubino and Hainbucher, 2007). To describe the ventilation of the Mediterranean Sea in terms of turnover times, residence times and mean ages, tracer measurements were carried out during the METEOR expedition M84/3 in 2011. The transient tracers Dichlorodi-

OSD
10, 1647–1705, 2013

fluoromethane (CFC-12) and Sulfur Hexafluoride (SF_6) as well as helium isotopes and tritium were measured to provide a comprehensive data set of time dependent tracers.

2 Materials and method

The expedition M84/3 from Istanbul to Vigo took place from the 5–28 April 2011 on the german research vessel FS Meteor (Tanhua et al., 2013a, b). Figure 1 shows an overview of the different sample stations separated in CFC-12, CFC-12 with isotopes and transient tracer stations including SF_6. The transient tracers CFC-12 and SF_6 were sampled at nearly all stations in the EMed whereas only three stations of SF_6 exist in the WMed. The measurements of CFC-12 and SF_6 were mainly performed on board. The water samples were taken with 250 mL glass syringes or 300 mL glass ampules under exclusion of atmosphere from niskin bottles whereat the sampling depths were chosen to cover the complete water column in a sufficient resolution. The syringes and ampules were stored in a cooling box filled with water of $\approx 0\,^{\circ}C$ to prevent outgasing of the tracers. The measurements were carried out with similar analytical systems as described by Bullister and Wisegarver (2008); Law et al. (1994). One measurement system named VS1 consisted of a Shimadzu GC14a gas chromatograph equipped with an Electron Capture Detector (ECD), stainless steel tubing system and Valco valves. The 1/8″ precolumn was packed with 30 cm *Porasil C*, the 1/16″ trap with 70 cm *Heysep D* and the 1/8″ main column with 180 cm *Carbograph 1AC* and a 20 cm *Molsieve 5 Å* tail-end. An evacuated vacuum sparge tower (VST) was used to transfer the water sample out of the glass ampule into the measurement system. Due to the low pressure in the VST, most of the dissolved gases pass over into the head space during the filling process. The residual was purged out with nitrogen in ECD-quality. The trap was installed in a Dewar filled with a bottom layer of liquid nitrogen. The distance between trap and cooling medium was regulated by a Lab Boy to hold a temperature range between $-70\,^{\circ}C$ to $-60\,^{\circ}C$ during the purge process. Due to some problems with the VS1 system and a sudden break down of the ECD several key stations have been flame

OSD
10, 1647–1705, 2013

sealed in glass ampules for a later onshore measurement. The sealed ampules were measured during summer 2011 at the IfM-GEOMAR in Kiel with the repaired VS1 instrument and an installed ampule cracker system similar to Vollmer and Weiss (2002).

The second measurement system PT3 consisted of a Shimadzu GC2014 gas chromatograph with a similar basic setup like the VS1 system but with a different column composition, sample chamber and trap system. The 1/8″ precolumn consisted of 60 cm *Porasil C* and 10 cm *Molsieve 5 Å*, the 1/8" main column of 180 cm *Carbograph 1AC* and 30 cm *Molsieve 5 Å*. Insufficient base line separation prevented a quantitative analysis of SF_6 with this column setup. For a measurement an aliquot of ≈ 200 mL was injected into the sample chamber with a sampling syringe and then also purged with highly purified nitrogen. Instead of a trap system with liquid nitrogen, a pressure regulated ethanol bath was used. The ethanol was cooled by a Julabo cooling finger to a minimum temperature of −68 °C. For the purge and trap process the fill level is raised until the trap dips into the ethanol and is lowered again for the heating process (Bullister and Wisegarver, 2008). The traps of both measurement systems were heated to 90 °C by an electrical current flow, which was automatically regulated by a Proportional-Integral-Derivative controller (PID). A detailed description of the data set, the sampling, the calibration and measuring procedure as well as a precise technical overview can be found in Stöven (2011).

The samples of tritium and helium-3 were measured by J. Sültenfuß at the Institute of Environmental Physics of the University of Bremen. Details of the measuring procedure and statistical evaluations can be found in Sültenfuß et al. (2009).

3 Transient tracers

3.1 Chronological transient tracers

The chronological transient tracers are based on an increasing tracer concentration in the atmosphere, thus a time varying source, like ChloroFluoroCarbons (CFC's) and

OSD
10, 1647–1705, 2013

SF_6. The concentrations of trace gases in the atmosphere are, for example, measured by the world wide AGAGE network, so that the input history over time is well known (Walker et al., 2000; Bullister, 2011). The production of CFC's and thus the emission was lowered and finally stopped in the late 80's respectively early 90's in the course of the Montreal Protocol which concerns of the handling of ozone depleting compounds. As a consequence, the concentration of CFC-12 currently decreases in the atmosphere, so that a cut-off limit of > 532 ppt in 2011 occurs. Every concentration above this limit describes two dates in the atmospheric history of the tracer shown in Fig. 2 and thus these CFC-12 concentrations are inconclusive for tracer age determination between 1994–2011. SF_6 has still an increasing concentration gradient but compared to the CFC's a very low emission rate. The recent concentration in the atmosphere is below 8 ppt but increasing roughly linearly. The production and use of SF_6 has partly local restrictions, but there is no international agreement yet despite of the high Global Warming Potential of 22 000 (IPCC, 1996). The tracers enter the oceans surface layer via gas exchange, following that the solubility is a function of temperature, salinity and the physical nature of the molecule. Such solubility functions like Eq. (1) are available for most of the CFC's and SF_6 (Warner and Weiss, 1985; Bullister et al., 2002).

$$\ln(F) = a_1 + a_2\left(\frac{100}{T}\right) + a_3 \ln\left(\frac{T}{100}\right) + a_4 \ln\left(\frac{T}{100}\right)^2 + S\left[b_1 + b_2\left(\frac{T}{100}\right) + b_3\left(\frac{T}{100}\right)^2\right] \quad (1)$$

The influence of wind speed, pressure and temperature drops in terms of under- or oversaturation is normally low and a saturation of 100 % is supposed to be correct. These solubility functions are used to convert the measured gravimetric units, e.g. pmol kg^{-1} for CFC-12 and fmol kg^{-1} for SF_6, into the partial pressure in ppt of a tracer. The partial pressure should be the preferred choice instead of the gravimetric units, because it is independent of pressure, salinity and temperature and thus directly com-

OSD
10, 1647–1705, 2013

parable within the complete water column and atmosphere. Chronological tracers are conserved tracers with no significant sources or sinks in the ocean interior. The concentration in the water column depends on the last time the water parcel was in contact with the atmosphere and of course also on the influence of mixing and diffusion.

3.2 Radioactive transient tracers

The radioactive tracers such as tritium and its decay product helium (^{3}He) form the second class of transient tracers. Tritium has a natural background concentration of $\approx$ 0.3 Tritium Units (TU) in the atmosphere, where 1 TU equals the number of one tritium atom per 10^{18} hydrogen atoms (Ferronsky and Polyakov, 1982). Due to nuclear bomb tests in the late 50s and 60s the tritium concentration increased up to 100 TU in the atmosphere and declined afterwards to a current concentration of 1–1.2 TU in 2011. The input of tritium into the ocean surface layer is a function of radioactive decay in the atmosphere, vapor pressure and the variance of location and extend of precipitation. Tritium decays to ^{3}He which equilibrates with the atmosphere as long as the water parcel remains in the boundary layer of gas exchange. Once the water reaches the ocean's interior, the radioactive decay serves as time varying sink.

The Mediterranean is characterized by higher tritium concentrations than the Atlantic due to continental influences in terms of weather conditions and fresh water input. A commonly used tritium input function (TIF) for the North Atlantic was obtained by Dreisigacker and Roether (1978) and further developed for the EMed by Roether et al. (1992). Based on this data set, another TIF for the EMed was created by R. Steinfeld (unpublished) where the data after 1974 was extrapolated by using the decay function of tritium. In the WMed the surface layer is mainly influenced by the inflow of Atlantic Water (AW), so that the input function needs to be corrected for the degree of dilution. The tritium stations of the M84/3 cruise can be used for a simple approach. Following that a correction factor can be calculated by the difference between the recent mean surface concentration of tritium in the WMed and the history suggested by R. Steinfeld (unpublished). The determined surface concentration are 15 % lower in the

OSD
10, 1647–1705, 2013

EMed and 35 % lower in the WMed than suggested in the original input function. Under the assumption that the determined offset is constant over years, both factors can be used as offset correction to create two alternative input functions (Fig. 3) which can be applied to a TTD mixing model, see below.

Figure 3 shows also the recent TIF of the Med by Roether et al. (2013), which also relies on the data set of Dreisigacker and Roether (1978). This TIF was recalculated for the EMed by using a dilution factor and mean surface tritium concentrations obtained during several cruises between 1974 and 2011. Comparing both recent TIFs of the EMed one can see that the shape of both curves are relatively similar. This points out that both input functions seem to be useful approaches for the EMed despite of the different buildup structure. However, by using an interpolated form of the input function of Roether et al. (2013) one yield higher mean ages compared to to the input function we obtained. The main deviation from the decay based input function is the data point of 1978 following that the interpolated tritium concentrations are significant elevated between 1975 and 1987, producing differences in mean ages. The mean deviation between the different TIFs and the original TIF of the North Atlantic are 86 % respectively 61 % (Roether et al., 2013) for the EMed and 43 % for the WMed.

4 Tracer age and the Transit Time Distribution

The age of a water parcel can be described in different ways. For chronological transient tracers the measured concentration of a sample c in year t_s can be set in relation to the concentration c_0 and year t_{hist} of the atmospheric history of the tracer (Eq. 2).

$$c(t_s) = c_0(t_{hist}) \quad (2)$$

The difference of the sampling year t_s and the obtained year t_{hist} defines the tracer age τ (Eq. 3).

$$\tau = t_s - t_{hist} \quad (3)$$

OSD
10, 1647–1705, 2013

The tracer age of radioactive tracers depends on first order kinetics shown in Eq. (4). The initial concentration $[A_0]$ and the decay constant λ are the required parameters to calculate the elapsed time of a tracer in a water parcel.

$$\tau = \frac{1}{\lambda} \cdot \ln\left(\frac{[A_0]}{[A]}\right) \tag{4}$$

As mentioned above, tritium has in addition to the radioactive decay a relevant input function and thus an unknown part for $[A_0]$. Therefore, the decay product of tritium needs to be measured. The tritiugenic ^{3}He replaces the initial concentration of tritium and Eq. (4) can be rewritten to Eq. (5). A generally accepted value for the decay constant of tritium is $\lambda = 0.05576\,/a$ (Unterweger et al., 1980; Taylor and Roether, 1982).

$$\tau = \frac{1}{\lambda} \cdot \ln\left(1 + \frac{\left[^3\mathrm{He}_{\mathrm{tri}}\right]}{\left[^3\mathrm{H}\right]}\right) \tag{5}$$

The significance of a tracer age is relatively low because it is based on the assumption of a complete advective behavior neglecting any diffusive mixing process. However, there are also some approaches like dilution models (Roether et al., 2013) and the tracer age of CFC-12 and SF_6 with a ≈ 14 yr time-lag (Tanhua et al., 2013c; Schneider et al., 2013) which allow an estimation of changes in ventilation. A model which accounts for mixing and diffusion is the Transit Time Distribution (TTD) model. The TTD is based on the Green's function and was invented to describe atmospheric ventilation processes (Hall and Plumb, 1994). However, the basic idea that a parcel of molecules changes its location under the influence of advection and diffusion can also be applied to ventilation processes of the ocean. Equation (6) is an analytical expression of the Green's function which provides access to use field data within the TTD model (Waugh et al., 2003). It is based on a one dimensional flow model with constant advective velocity and diffusivity and is therefore known as the one dimensional Inverse Gaussian

OSD
10, 1647–1705, 2013

Transit Time Distribution (1D-IG-TTD).

$$G(t) = \sqrt{\frac{\Gamma^3}{4\pi\Delta^2 t^3}} \cdot \exp\left(\frac{-\Gamma(t-\Gamma)^2}{4\Delta^2 t}\right) \quad (6)$$

The key variables in this equation are Γ for the mean age and Δ for the width of the distribution. The age spectra t is defined by the initial year t_i of the atmospheric history respectively the input function of the tracer and the year of sampling t_s. Equation (7) shows for example the time range of CFC-12 for the sampling year 2011.

$$t_{\text{CFC-12}} = 1936(t_i)\ldots 2011(t_s) \quad (7)$$

To give a statement on the share of advection and diffusion the Δ/Γ ratio can be used. A low ratio like 0.4–0.8 indicates a high advective part e.g. extensive deep water formations whereas a high ratio like 1.2–1.8 indicates a more diffusive character of the water parcel. The definite integral of Eq. (8) contains the link between the measured concentration of a sample $c(ts)$ and the mean age of the TTD.

$$c(t_s) = \int_0^\infty c_0(t) \cdot G(t)\mathrm{d}t \quad (8)$$

A further approach to determine a mean age is the linear combination of two distributions which is shown in Eq. (9). Similar to an one Inverse-Gaussian-TTD, a possible solution is a two Inverse-Gaussian-TTD (1D-2IG-TTD) and can be envisioned for two water masses with different histories (age), but with similar density, that mixes in the ocean interior. This model has been explored by, for instance, Waugh et al. (2002).

$$c(t_s) = \int_0^\infty c_0(t) \cdot [\alpha\ G(\Gamma_1, \Delta_1, t) + (1-\alpha)\ G(\Gamma_2, \Delta_2, t)]\mathrm{d}t \quad (9)$$

OSD
10, 1647–1705, 2013

The number of possible combinations of distributions and parameters provides a comprehensive concept of age modeling in the ocean. The main complexity consists of finding accurate and reasonable solutions fitting to the field data. The mean age is then determined by Eq. (10).

$$\Gamma = \alpha \cdot \Gamma_1 + (1 - \alpha) \cdot \Gamma_2 \quad (10)$$

5 Practical application of the TTD model

A common procedure described in several published articles (e.g., Schneider et al., 2010; Waugh et al., 2006, 2004) is to apply the 1IG-TTD with a ratio of $\Delta/\Gamma = 1$ to the tracer data to calculate a water mass mean age. The Δ/Γ has been demonstrated to be close to one in large parts of the world ocean. This might be a helpful and sufficient approach where data of only one tracer exists. Furthermore, a TTD related approach of age spectra modeling was carried out by Steinfeldt (2004) for the EMed in 1987. Another reasonable case is to analyze transient tracer time series in terms of changes in ventilation where the rate of age growth per year is more in focus than a precise mean age (Huhn et al., 2013). Furthermore the standard procedure should be used within tracer surveys with few sample points because local outliers of constrained data points can produce significant flaws in interpolation. For a comprehensive data set, consisting of more than one transient tracer, a constrained TTD model should be the preferred choice. The determined Δ/Γ ratios provide a first insight into the water mass structure concerning the advective and dispersive behavior. The further analysis of ventilation processes and recent changes in water masses as well as the estimation of the anthropogenic carbon column inventory is based on the determined mean age and thus dependent on the exact Δ/Γ ratio.

OSD
10, 1647–1705, 2013

5.1 Constraining the IG-TTD model

The prerequisite to constrain the IG-TTD is a transient tracer couple. The tracers of the couple need to have sufficiently different atmospheric histories to constrain the Δ/Γ ratio. For tracer couples with quite similar atmospheric histories like CFC-12 and CFC-11 one yield a wide range of possible solutions and thus a non-constrained TTD. Useful couples are CFC-12/SF_6 and tritium/SF_6. The first step of data processing includes the calculation of mean ages for Δ/Γ ratios between 0.0–1.8 for every data point and tracer, always taking into account the correct surface ocean history of the source region. The determined data points of mean age vs. Δ/Γ ratio are used to obtain polynomial regressions of second order. Following that every sample point of every tracer can be expressed by a mean age function (Eq. 11).

$$\Gamma = a\left({}^{\Delta}/_{\Gamma}\right)^2 + b\left({}^{\Delta}/_{\Gamma}\right) + c \tag{11}$$

The intersection between two mean age functions denotes the constrained Δ/Γ ratio and mean age. In some cases where no exact intersection can be found it is useful to determine the local minimum of a combined mean age function in the range of Δ/Γ. A local minimum indicates the point of the smallest difference in mean ages, which should be used to a maximum difference of 5 yr to ensure also the consideration of a maximum analytical error of $\approx 4\,\%$. To obtain the mean age of such a minimum function, the average of both mean ages needs to be calculated. However, in some cases it is more meaningful to use one of the tracer mean ages than the average mean age. For example are SF_6 mean ages for recently ventilated waters more significant than CFC-12 mean ages. In contrast, CFC-12 mean ages should be used in older water layers where SF_6 concentrations are close to the detection limit.

A further aspect of the IG-TTD model is the validity area of each tracer couple, which defines the possible range of IG-TTD solutions. A rough classification of the specific validity area of a couple can be done by determining the tracer age differences. For example, if the difference in tracer ages between SF_6 and CFC-12 is large (10 yr for

OSD
10, 1647–1705, 2013

the sampling year of 2011), it indicates that a 1IG distribution cannot explain the tracer distribution, and more refined models of the TTD are needed, for instance the linear combination of two IG-TTDs.

5.2 Constraining the 2IG-TTD model

Due to the five free parameters α, Γ_1, Γ_2, Δ_1 and Δ_2 the system of equations is under-determined for any tracer survey with less than five measured transient tracers. Most surveys include two or three transient tracers with sufficiently differences in atmospheric histories. Here we introduce one way to use an under-determined 2IG-TTD model. Based on oceanographic water mass analysis one can estimate the composition of the current state of the water masses and roughly the underlying mixing processes. As described above the Western and Eastern Mediterranean are both affected by an extensive deep water formation with fresh and salty water from the surface and intermediate layer respectively. The null hypothesis is that an old and more stationary water mass can be described by a 1IG-TTD which is or was intruded by a younger water parcel described by another 1IG-TTD. Hereby the younger water parcel might be characterized by a more advective behavior with a low ratio, e.g. $\Delta/\Gamma = 0.6$. The ratio of the more stationary water mass is set to $\Delta/\Gamma = 1.4$, describing a typical ratio of a more diffusive/dispersive behavior. By making assumptions about the Δ/Γ ratio of both 1IG-TTDs one can calculate mean age matrices for different α's with $x = \Gamma_1$, $y = \Gamma_2$ and $z = C_{\text{tracer}}$. The concentration of a measured sample generates different concentration curves for each α in the xy-plane (Fig. 4). The predefined 2IG-TTD is constrained if there is an intersection area of the concentration curves of different tracers describing one mean age (Eq. 10).

OSD
10, 1647–1705, 2013

6 Results and discussion

6.1 General ventilation pattern

6.1.1 Eastern Mediterranean Sea

The zonal sections of the transient tracer concentrations of the Ionian and Levantine Sea show some significant characteristics of their ventilation (Fig. 5, 6). Between 27° E and the coast of Lebanon a clear Tracer Minimum Zone (TMZ) can be identified by all three tracers which vertically spreads approximately from 700–1600 m depths. The core concentration of the TMZ is 106 ppt for CFC-12, 0.3 ppt for SF_6 and 0.3 TU for tritium whereat the lowest values are not visible in the gridded fields shown in Fig. 6. Beneath this TMZ the tracer concentrations are elevated in the deep water due to the deep water formation in the Eastern Mediterranean Sea that led to a high volume input of tracer rich and dense water masses. The bottom concentration of the tracers are $\approx$ 200 ppt for CFC-12, $\approx$ 1.1 ppt for SF_6 and $\approx$ 0.6 TU for tritium. In the westerly parts of the section (i.e. the deep Ionian Sea) the tracer concentration is higher in the deep and bottom layer than in the east. This water mass characteristic belongs to recent intrusions of ASOW coming from the deep water source in the Adriatic Sea. Station 313 in the Adriatic Pit can be used as representative example for the source region of the ASOW. The concentration profiles show, that the Adriatic Pit is a well mixed and ventilated basin with minimum tracer concentrations of CFC-12 > 429 ppt, SF_6 > 5 ppt and tritium > 0.9 TU (Fig. 7). The high concentrations of CFC-12 and tritium throughout the whole water column at station 288 in the Cretan Sea can be related to the time range between 1990s until today (Fig. 8). The concentration gradient of SF_6 indicates a recent return to a more layered structure in the Cretan Sea, following that the high concentrations of CFC-12 and tritium in the intermediate and deep water have to be formed before this layering process, probably during the 1990s. This would imply that the EMT source region was a complete mixed basin during the outflow event. The difference in tracer structures is related to the increasing input function of SF_6 and the

OSD
10, 1647–1705, 2013

weak input functions of CFCs since early 1990s, i.e. the onset of the EMT. CFC-12 and tritium concentrations cannot be used to identify the recent change in ventilation of the Cretan Sea. A further aspect is the distribution of SF_6 in the Ionian and Levantine Sea which looks more homogeneous in the intermediate and deep water compared to CFC-12. This is based on the relatively young atmospheric history of SF_6, following that the deep water masses are less effected by this tracer. Accurate measurements between 1 ppt and the detection limit are needed to have an useful resolution. As mentioned above, CFC-12 has a long atmospheric history with a rapid concentration increase over several decades. Thus, CFC-12 has a large dynamic scale within the measurement range, so that CFC-12 is an important tracer for intermediately old water masses.

6.1.2 Western Mediterranean Sea

The CFC-12 and tritium section from the Tyrrhenian Sea through the Western Basin into the Alboran Sea show, that the Western Mediterranean Deep Water (WMDW) is completely intruded by recently ventilated water masses coming from the extensive deep water formation during 2004–2006 (Fig. 5, 9, 10) (Schroeder et al., 2008, 2010). The CFC-12 concentrations are > 260 ppt and the tritium concentrations are > 0.5 TU throughout the whole bottom layer of the Western Basin reaching the channel between Sardinia and Sicily (Fig. 9, 10). Figure 11 shows in detail that newly formed WMDW starts to enter the Tyrrhenian Sea along this bottom contour without reaching the interior water masses in 2011. The Tyrrhenian Sea is characterized by CFC-12 concentrations below 180 ppt and tritium concentrations < 0.5 TU suggesting that this basin was not effected by input of the 2004–2006 deep water formation into the deep and bottom water layers by 2011. These relatively low tracer concentrations from the Tyrrhenian Basin rudimentary extends as tongue into the intermediate layer between 700–1300 m of the Western Basin which correlates with the results of Rhein et al. (1999).

OSD
10, 1647–1705, 2013

6.2 Transit Time Distributions

6.2.1 1IG-TTD

The first approach of mean ages is based on the obtained Δ/Γ ratios for the 1IG-TTD model which also provide further information on water mass characteristics. For samples of the EMed the major share of Δ/Γ ratios was determinable for the CFC-12/SF_6 tracer couple in a reasonable range. Figure 12 shows the section of Δ/Γ ratios as interpolated macrostructure in the EMed based on CFC-12 and SF_6 and the 1IG-TTD model. The sectional interpolation quality is reduced due to non constrainable data points. Figure 12 indicates that the TMZ spreading is more effected by the EMT event than the tracer concentrations suggest. The water below 1200 m in the Levantine Basin have ratios between 0.4 to 0.6 indicating a high advective behavior of the EMT event. The TMZ has ratios between 1.0 to 1.3 as expected for a stable water mass where diffusion predominates. The low Δ/Γ ratios of the EMT water masses are also observed in the easterly deep waters of the Ionian Sea whereas the deep waters further west formed by ASOW have ratios between 1.2–1.4. Combining the second tracer couple consisting of SF_6 and tritium with the corrected input function one yield a similar trend of Δ/Γ ratios in the EMed (Fig. 13). However, there are only four stations with tritium measurements available within the section of the EMed (290, 292, 301, 305) and thus the sectional interpolation is restricted to 34 data points which does not allow a resolution of local phenomena but only provides a rough overview.

Comparing the Δ/Γ ratios in the intermediate and deep water layers of the Cretan Sea (Fig. 14) with the EMT water masses in the Ionian and Levantine Sea (Fig. 12), one can see that the formation of the Cretan Sea Overflow Water (CSOW) as well as the EMT event itself were based on distinctly advective processes with expected mean ages nearby the tracer ages. In contrast, water masses coming from Adriatic Deep Water (ADW) seems to be formed by water masses with a more dispersive character belonging to slower formed water layers indicated by significant high Δ/Γ ratios between 1.1–1.6 (Fig. 15), whereat the red dots in Fig. 15 indicate non-constrained data

OSD
10, 1647–1705, 2013

points with a mean age difference between 6–25 yr. One can suppose that the formation of ASOW is based on slower dispersive processes of different water masses. The westerly bottom water of the Ionian Sea show the same dispersive characteristics as the ASOW (Fig. 12). This indicates that both states of Δ/Γ ratios were mainly defined by the formation process of ASOW/CSOW source water and only in minor share by mixing processes along the current pathway from source region into the interior of the Levantine and Ionian Sea. Therefore, the transient tracer concentrations of both deep water masses are not necessarily simply indicators of their ventilation.

Figures 16 and 17 show the determined mean ages constrained by either CFC-12 and SF_6 or tritium and SF_6. The tritium/SF_6 based maximum mean age of the TMZ in the Levantine Sea is 260 yr and the deep and bottom water have mean ages between 70–80 yr. In contrast, the CFC-12/SF_6 based maximum mean age of the TMZ is 230 yr with further high mean ages in the Ionian Sea between 120–180 yr. The deep and bottom water from the EMT event is the youngest water with mean ages between 50–80 yr. Station 290 which is near the overflow area of the CSOW which can be seen by the young EMT mean ages up to the intermediate layers. The deep water in the Ionian Basin has a mean age of 100 yr which underlines the difference of both deep water formations: Although the Adriatic deep water formation is contemporary and the EMT event replenished large parts of the deep waters in the early 1990s, the deep water layer formed by water masses from the Cretan Sea is much younger than the one from the Adriatic Sea. The mean ages of both source regions are quite young with maximum mean ages in the deep water of ≈ 20 yr in the Aegean Sea, which highly correlates with the timing of the EMT event in the early 1990s, and $\approx 10-17$ yr in the Adriatic Sea (Fig. 18, 19). The mean age gradient with depth is much steeper in the Adriatic Sea than in the Cretan Sea which also show that the ventilation processes of both basins are significantly different. However, the SF_6 mean ages indicated by red dots in Fig. 19 at station 313 in the Adriatic Sea fit into the mean age gradient, even though this mean ages are based on minimum functions with a mean age difference of more than 5 yr. Such data points are defined as non-constrained, despite of possible true solutions for

OSD
10, 1647–1705, 2013

one transient tracer, and should not be used due to the uncertainty by using different transient tracers with the same "approached" constraints. Figures 20 and 21 show the mean age functions of CFC-12 and SF_6 including the analytical error range of 4 %. Figure 20 shows an example of the Cretan Sea deep water and Fig. 21 of the Adriatic Sea deep water. Both plots show the differences in water mass structure, in terms of advective/diffusive ratios, despite of uncertainties in the mean age calculations.

Neglecting any systematic errors in sampling and measurements, the ages of a TTD model are strongly influenced by the atmospheric history respectively the input function of a transient tracer. The atmospheric histories of CFC-12 and SF_6 are very well known and the data can be used for every survey region due to the fast atmospheric mixing. However, the input function of tritium in the Mediterranean is much more complex. The regional impact of tritium concentrations in precipitations and local transport processes is mostly unknown so that the obtained input function of tritium by Dreisigacker and Roether (1978) and Roether et al. (1992) is a rough estimate of a mean input of tritium into the surface layer of the ocean. Nevertheless, this input function is the best existing approach and the results of the offset corrected input function clearly show that the shape of the curve tends to be correct. The corrected input function of the EMed generates similar but still slightly higher mean ages compared to the ones obtained by CFC-12 and SF_6 (Fig. 16). This indicates that the corrected input function probably still over estimates the mean input of tritium in the Eastern Mediterranean Sea. The 1IG-TTD provides significant results for the EMed using the tracer couple of CFC-12 and SF_6, whereas SF_6 and tritium should be used with some caution.

The analysis of Δ/Γ ratios in the WMed is restricted to only three stations (317, 323, 334) for which the concentration ratios between the two transient tracer couples were not usable with the 1IG-TTD model. The simple approach of water mass analysis concerning the advective/diffusive ratio and the calculation of mean ages is not possible. Another distribution model is needed to estimate mean ages of non constrainable data points of both tracer couples in the Western Mediterranean Sea. Figure 22 shows the approach of the validity area by using the tracer age differences of SF_6 and CFC-12

OSD
10, 1647–1705, 2013

in the EMed. The young and advective EMT water mass can be described by the 1IG-TTD, whereas the mean ages of the intermediate water and parts of the deep water in the EMed as well as the complete WMed might be better evaluated by a 2IG-TTD. The limiting difference also depends on the tracer concentration to some extend. Following that the mixed layer and parts of the pycnocline can also be described by the 1IG model, although the tracer age difference is larger than 10 yr. To develop a clear mathematical definition of validity areas of different tracer couples and distribution models will be part of future work.

6.2.2 2IG-TTD

The predefined 2IG-TTD was applied to several key stations in the EMed and WMed (290, 305, 317, 323) shown in Fig. 5. As mentioned above we assumed fixed Δ/Γ ratios for both TTDs so that $\Delta_1/\Gamma_1 = 1.4$ and $\Delta_2/\Gamma_2 = 0.6$, respectively and that the mean ages $\Gamma_2 < \Gamma_1$ under the assumption that Γ_2 describes the younger water parcel. The concentration curve (Fig. 4) of each transient tracer were combined in one matrix to determine the intersections. The weighting factor α was separated in 10 % steps and thus one yield eleven concentration matrices for each sample point. The determination of the intersections was carried out numerically to obtain a first overview of possible 2IG-TTD results which are shown in Table 1–4 where the mean ages are based on the concentrations of CFC-12, SF_6 and to some extent also tritium, see discussion below.

Station 290 in the Levantine Sea can be perfectly described by the 1IG-TTD which is also indicated by the 2IG-TTD results. As shown in Table 1 the best fits for all samples are obtained for $\alpha = 0$ which is the lower limiting case where the 2IG-TTD turns into a 1IG-TTD with $\Gamma = \Gamma_2$. Hence, the mean ages of the 2IG-TTD are the same as the ones from the constrained 1IG-TTD where $\Delta/\Gamma = 0.6$. The missing data in Table 1 corresponds to the mean ages of 1IG-TTD's with Δ/Γ ratios < 0.6. Figure 23 shows the characteristics of such a concentration curve plot. For $\alpha = 0$ the lines of CFC-12 and SF_6 are overlapping, whereas the one of tritium is slightly above, again indicating a higher mean age by this tracer. The changes of the concentration curves with in-

OSD
10, 1647–1705, 2013

creasing α are of different extend. The rate of change is highest for tritium, followed by CFC-12 and lowest for SF_6. This means that one can expect curve intersections under the condition of $\Gamma_2(\text{Tritium}) > \Gamma_2(\text{CFC-12}) > \Gamma_2(SF_6)$ at $\alpha = 0$.

This condition can be found at station 305, which is a key station in the Ionian Sea where the 1IG-TTD is less constrainable in the intermediate and deep water. However, CFC-12 and SF_6 intersect each other for several choices of alpha, so we choose the one with the lowest difference to the tritium intersection (Fig. 24). Table 2 shows the results of the 2IG-TTD for station 305. The intermediate and deep water is characterized by high α values between 80–90 % indicating a stronger influence of more stationary water masses. Looking at the single results of the two mean ages of the distribution, the total mean age is mainly influenced by Γ_1 rather than Γ_2, whereat these single results are not significant for statements about real mixing processes. They are rather part of the predefined model characteristics and provide only tendencies of the water mass behavior. Whereas the total mean age from the constrained and exact determined TTD model describes the solved equation and thus a significant form of age of a water parcel. The highest mean age of 260 yr can be found at ≈ 1000 m depth, whereas the mean age decreases to 90 yr at the bottom layer. This is in full compliance with the expected younger water masses belonging to the ASOW. Compared to the 1IG-TTD, which indicates a mean age of 100 yr for most of the water column, the 2IG-TTD shows a more differentiated structure with a clear mean age maximum. Indicating that in this case the 2IG-TTD provides more reasonable results.

The order of tracer mean ages at station 317 in the Tyrrhenian Sea changes from the required standard condition into $\Gamma_2(\text{CFC-12}) > \Gamma_2(\text{Tritium}) > \Gamma_2(SF_6)$ for depths shallower than 1250 m. This change in order is also the limit of the used model following that only four samples could be determined in the Tyrrhenian Sea (Tab. 3). The mean ages are ≈ 200 yr in the deep water and increase up to 531 yr at 1250 m. The Tyrrhenian Sea is less affected by intrusion of younger water masses and thus one would expect this high mean ages in this basin. There might be several reasons why the major part of the mean age is not determinable in the Tyrrhenian Sea. The values for

OSD
10, 1647–1705, 2013

Γ_1 are increasing with decreasing depth up to 757 yr. The used mean age matrices have a size of 1000 × 200 following that a maximum mean age of 1000 yr can be determined for Γ_1. The shape of the curves of CFC-12 and SF_6 show the tendency to have intersections beyond this limit and thus much higher mean ages for Γ_1 than 1000 yr. Another possible reason might be the assumed values of Δ/Γ ratios of the 2IG-TTD. With bigger mean age matrices or different choices of parameters the mean age should be also determinable in this part of the Mediterranean Sea.

Station 323 in the Alghero–Provençial Basin shows significant characteristics of the newly formed deep and bottom water layer with a constant α of 60 % and mean ages between 170–250 yr (Table 4, Fig. 25). The lower values of α besides relatively high mean ages describe the extensive intrusion of young water masses into an old deep water layer. The interbasin circulation pattern between the Alghero–Provençial Basin and the Tyrrhenian Sea is characterized by high α values denoting less influence of advective water mass input at depth between 1500–800 m. However, the mean ages are relatively lower at this depth range than one would expect at station 323. Even though the massive inflow of recently ventilated water of 2004–2006 might have notably lowered the mean age, one can still find the oldest water masses in the deep and bottom water. Suggesting that these water layers of the Western Basin were probably less mixed over decadal to centennial time scales. This illustrates the power of the 2IG-TTD approach: whereas the 1IG-TTD and tracer age concepts both indicates the oldest waters at intermediate depths (e.g., Rhein et al., 1999; Schneider et al., 2013), our analysis show the highest mean ages in the deep water.

6.3 Best mean age approach

Figure 26 shows the mean age section in the EMed based on the combination of both TTD models. For non constrainable data points within the 1IG-TTD the predefined 2IG-TTD was used to calculate the mean ages. This cross-interlocking of both models provides the best estimate of mean ages in the eastern part of the Mediterranean Sea. One can clearly see the young water masses of the EMT event in the deep and bottom

OSD
10, 1647–1705, 2013

layers of the Levantine and Ionian Basin with mean ages between 60–80 yr and the newly formed deep water in the westerly parts of the Ionian Basin with mean ages between 120–160 yr. The mean age maximum layer extends from 600 m to 2000 m depth throughout the whole EMed withmean ages between 160–290 yr. The maximum mean age of 290 yr can be found in the TMZ in the Levantine Sea. This high mean age layer is disrupted by lower mean ages of ≈ 140 yr at the outflow areas of the Cretan Sea (station 299 and 290) as well as in the area near Rhodes (station 293) also with mean ages of ≈ 140 yr.

7 Conclusions

We have described a comprehensive set of transient tracer data sampled during the Meteor 84/3 cruise through the Mediterranean Sea in April 2011. For the first time measurements of SF_6, CFC-12, tritium and ^{3}He were performed simultaneous on a cruise covering all major basins of the Mediterranean Sea. With this data set we constrain ventilation characteristics using the Transit Time Distribution (TTD) framework. In particular we constrain the TTD assuming Inverse Gaussian (IG) shape of the TTD, either as an one (1IG) or two-modal (2IG) distribution. The shape-determining parameters of the IG distribution are the width (Δ) and mean age (Γ), the relative contribution of the two water-masses of a 2IG distribution (α), as well as the ratio of Δ/Γ that is indicative of the diffusive to advective transport characteristic of a water mass.

Most parts of the EMed can be described by the 1IG-TTD model but with widely different Δ/Γ characteristic of the two main deep-water sources, the Cretan Deep Water (CDW) and the Adriatic Sea Overflow Water (ASOW), that have developed already their origin region rather than along the flow pathway. The Aegean Sea source water shows a more advective (i.e. a low Δ/Γ ratio) behavior than the Adriatic Sea source water that have a more diffusive behavior. The majority of the deep water in the Eastern Mediterranean of Aegean Source originates from the Eastern Mediterranean Transient (EMT) event in the early 1990s. The unusually high deep-water formation rates during

OSD
10, 1647–1705, 2013

this event might explain the advective characteristics of this water-mass, having a mean age between 50 and 80 yr. The mean ages of the EMT-induced water masses in the Levantine Basin are thus still younger than the deep water in the deep Ionian Sea that has mean ages of approximately 120–160 yr using the 2IG TTD model. This is, at first sight, counter-intuitive considering the higher CFC-12 concentration in the deep Ionian Sea due to recent contribution from the deep water source in the Adriatic Sea, compared to the Levantine Basin. All tracers show a distinct minimum at around 1000 m depth throughout the Med, although the origin of this Tracer Minimum Zone (TMZ) is slightly different for the eastern and western basins. For the EMed horizontal gradients in the Δ/Γ ratio lead to a mean age distribution that is not directly correlated to the tracer concentrations, with lower mean ages southeast of Crete, in the outflow region of water from the Cretan Sea, and higher ages in the Levantine Basin and Ionian Sea.

Although most of the EMed ventilation can be described by a 1IG-TTD model, there are areas where this model of mixing cannot explain the observed tracer distributions. We found the 1IG-TTD approximation to be invalid for water samples with a tracer-age difference exceeding $\approx$ 10 yr (for the SF_6-CFC-12 couple sampled in 2011). Thus we use a 2IG model to constrain the TTD in the western part of the Ionian Sea and most of the WMed. The Western Mediterranean Transition (WMT) event with enhanced deep-water formation during the winters of 2004–2006 in the Western Basin can be characterized by the 2IG-TTD model, where the recently ventilated deep-water with advective properties mixes with more stationary water of more diffusive character. The contemporaneous deep water in WMed has approximately 40% contribution of recently ventilated waters from the WMT, leading to mean ages of about 200 yr, which is similar or higher than the mean ages higher up in the water column that have lower CFC-12 and SF_6 concentrations. This highlights the need to constrain the TTD in order to understand the "age" of a water mass based on transient tracer concentrations. The recently ventilated deep water was observed as elevated concentrations of CFC-12 in excess of 200 ppt along the bottom in the Sardinia Channel towards, but not yet within, the Tyrrhenian Sea. The horizontally relatively homogeneous CFC-12 concentration of

OSD
10, 1647–1705, 2013

the Western Basin suggest that the TTD structure determined at station 323, SW of Sardinia, can be extrapolated to large parts of the WMed.

The results presented here points to the need to consider alternatives to the commonly applied 1IG-TTD model, particularly in regions with variable ventilation or where more water masses mix with each other. For observational constrains of more complex TTDs, a suite of transient tracers needs to be measured and interpreted. For such regions in the ocean, we show that a predefined 2IG-TTD provides a useful tool.

Acknowledgements. The authors want to thank the captain and crews on the research vessels Meteor for the excellent cooperation during the campaign. The Meteor cruise M84/3 and the transient tracer measurements were supported by a grant from the Deutsche Forschungsgemeinschaft-Senatskommission für Ozenographie (DFG), and from a grant from the DFG; TA 317/3-1. Furthermore we would like to thank Wolfgang Roether for his support, help and inspiring discussions of particular matters of helium and tritium.

The service charges for this open access publication have been covered by a Research Centre of the Helmholtz Association.

References

Artegiani, A., Bregant, D., Paschini, E., Pinardi, N., Raicich, F., and Russo, A.: The Adriatic Sea General Circulation, Part I: air-sea interactions and water mass structure, J. Phys. Oceanogr., 27, 1492–1514, 1996a. 1650

Artegiani, A., Bregant, D., Paschini, E., Pinardi, N., Raicich, F., and Russo, A.: The Adriatic Sea General Circulation, Part II: baroclinic circulation structure, J. Phys. Oceanogr., 27, 1515–1532, 1996b. 1650

Brasseur, P., Beckers, J., Brankart, J., and Schoenauen, R.: Seasonal temperature and salinity fields in the Mediterranean Sea: climatological analyses of a historical data set, Deep-Sea Res. Pt. I, 43, 159–192, 1996. 1649

OSD
10, 1647–1705, 2013

Bullister, J. L.: Atmospheric CFC-11, CFC-12, CFC-113, CCl4 and SF6 Histories (1910–2011), Carbon Dioxide Information Analysis Center, available at: http://cdiac.ornl.gov/oceans/new_atmCFC.html, 2011. 1653

Bullister, J. L. and Wisegarver, D.: The shipboard analysis of trace levels of sulfur hexafluoride, chlorofluorocarbon-11 and chlorofluorocarbon-12 in seawater, Deep-Sea Res. Pt. I, 55, 1063–1074, 2008. 1651, 1652

Bullister, J., Wisegarver, D., and Menzia, F.: The solubility of sulfur hexafluoride in water and seawater, Deep-Sea Res. Pt. I, 49, 175–187, 2002. 1653

Dreisigacker, E. and Roether, W.: Tritium and ^{90}Sr in North Atlantic surface water, Earth Planet. Sc. Lett., 38, 301–312, 1978. 1654, 1655, 1665

Ferronsky, V. and Polyakov, V.: Environmental Isotopes in the Hydrosphere, John Wiley & Sons, Chichester, New York, 1982. 1654

Hainbucher, D., Rubino, A., and Klein, B.: Water mass characteristics in the deep layers of the western Ionian Basin observed during May 2003, Geophys. Res. Lett., 33, L05608, 2006. 1650

Hall, T. and Plumb, R.: Age as a diagnostic of stratospheric transport, J. Geophys. Res., 99, 1059–1070, 1994. 1656

Huhn, O., Rhein, M., Hoppema, M., and van Heuven, S.: Decline of deep and bottom water ventilation and slowing down of anthropogenic carbon storage in the Weddell Sea, 1984–2011, Deep-Sea Res. Pt. I, 76, 66–84, doi:10.1016/j.dsr.2013.01.005, 2013. 1658

IPCC: Radiative Forcing of Climate Change, Report of the Scientific Assessment Working Group of IPCC, in: Climate Change 1995, The Science of Climate Change, edited by: Houghton, J. T., Meira Filho, L. G., Callander, B. A., Harris, N., Kattenberg, A., and Maskell, K., Cambridge University Press, Cambridge, UK, 1996. 1653

Klein, B., Roether, W., Manca, B., Bregant, D., Beitzel, V., Kovacevic, V., and Luchetta, A.: The large deep water transient in the eastern Mediterranean, Deep-Sea Res. Pt. I, 46, 371–414, doi:10.1016/S0967-0637(98)00075-2, 1999. 1649, 1650

Lascaratos, A., Williams, R., and Tragou, E.: A Mixed-Layer Study of the Formation of Levantine Intermediate Water, J. Geophys. Res., 98, 14739–14749, 1993. 1649

Lascaratos, A., Roether, W., Nittis, K., and Klein, B.: Recent changes in deep water formation and spreading in the eastern Mediterranean Sea: a review, Prog. Oceanogr., 44, 5–36, doi:10.1016/S0079-6611(99)00019-1, 1999. 1649

OSD
10, 1647–1705, 2013

Law, C., Watson, A., and Liddicoat, M.: Automated vacuum analysis of sulphur hexafluoride in seawater: derivation of the atmospheric trend (1970–1993) and potential as a transient tracer, Mar. Chem., 48, 57–69, 1994. 1651

Malanotte-Rizzoli, P. and Hecht, A.: Large scale properties of the eastern Mediterranean: a review., Oceanol. Acta, 11, 323–335, 1988. 1649

Rhein, M., Send, U., Klein, B., and Krahmann, G.: Interbasin deep water exchange in the western Mediterranean, J. Geophys. Res. Oceans, 104, 23495–23508, doi:10.1029/1999JC900162, 1999. 1662, 1668

Roether, W. and Schlitzer, R.: Eastern Mediterranean deep water renewal on the basis of chlorofluoromethane and tritium data, Dynam. Atmos. Oceans, 15, 333–354, 1991. 1650

Roether, W., Schlosser, P., Kuntz, R., and Weiss, W.: Transient-tracer studies of the thermohaline circulation of the Mediterranean, Reports in Meteorology and Oceanography, 41, 291–317, 1992. 1654, 1665

Roether, W., Manca, B., Klein, B., Bregant, D., Georgopoulos, D., Beitzel, V., Kovacevic, V., and Luchetta, A.: Recent changes in eastern Mediterranean deep waters, Science, 271, 333–335, 1996. 1649

Roether, W., Klein, B., Beitzel, V., and Manca, B.: Property distributions and transient-tracer ages in Levantine intermediate water in the eastern Mediterranean, J. Marine Syst., 18, 71–87, 1998. 1649

Roether, W., Jean-Baptiste, P., Fourrè, E., and Sültenfuß, J.: The transient distribution of nuclear weapon-generated tritium and its decay product ^{3}He in the Mediterranean Sea, 1952–2011, and their oceanographic potential, Ocean Sci., 10, 649–690, doi:10.5194/osd-10-649-2013, 2013. 1655, 1656, 1682

Rubino, A. and Hainbucher, D.: A large abrupt change in the abyssal water masses of the eastern Mediterranean, Geophys. Res. Lett., 34, L23607, doi:10.1029/2007GL031737, 2007. 1650

Schlitzer, R., Roether, W., Oster, H., Junghans, H., Hausmann, M., Johannsen, H., and Michelato, A.: Chlorofluoromethane and oxygen in the eastern Mediterranean, Deep-Sea Res. Pt. I, 38, 1531–1551, 1991. 1650

Schneider, A., Tanhua, T., Koertzinger, A., and Wallace, D.: High anthropogenic carbon content in the eastern Mediterranean, J. Geophys. Res., 115, C12050, doi:10.1029/2010JC006171, 2010. 1658

OSD
10, 1647–1705, 2013

Schneider, A., Tanhua, T., Roether, W., and Steinfeldt, R.: Changes in ventilation of the Mediterranean Sea during the past 25 yr, Ocean Sci., 10, 1405–1445, doi:10.5194/osd-10-1405-2013, 2013. 1656, 1668
Schroeder, K., Gasparini, G., Tangherlini, M., and Astraldi, M.: Deep and intermediate water in the western Mediterranean under the influence of the eastern Mediterranean Transient, Geophys. Res. Lett., 33, L21607, doi:10.1029/2006GL027121, 2006. 1649
Schroeder, K., Ribotti, A., Borghini, M., Sorgente, R., Perilli, A., and Gasparini, G.: An extensive western Mediterranean deep water renewal between 2004 and 2006, Geophys. Res. Lett., 35, L18605, doi:10.1029/2008GL035146, 2008. 1649, 1662
Schroeder, K., Josey, S., Herrmann, M., Grignon, L., Gasparini, G., and Bryden, H.: Abrupt warming and salting of the western Mediterranean Deep Water after 2005: atmospheric forcings and lateral advection, J. Geophys. Res., 115, C08029, doi:10.1029/2009JC005749, 2010. 1649, 1662
Steinfeldt, R.: Ages and age spectra of eastern Mediterranean Deep Water, J. Mar. Syst., 48, 67–81, 2004. 1658
Stöven, T.: Ventilation processes of the Mediterranean Sea based on CFC-12 and SF_6 measurements, GEOMAR OceanRep, diploma thesis, Christian-Albrechts-Universität zu Kiel, Kiel, 2011. 1652
Sültenfuß, J., Roether, W., and Rhein, M.: The Bremen mass spectrometric facility for the measurement of helium isotopes, neon, and tritium in water, Isot. Environ. Health Stud., 45, 1–13, 2009. 1652
Tanhua, T., Hainbucher, D., Cardin, V., Alvarez, M., and Civitarese, G.: Repeat hydrography in the Mediterranean Sea, data from the Meteor cruise 84/3 in 2011, Earth Syst. Sci. Data, 5, 289–294, doi:10.5194/essd-5-289-2013, 2013. 1651
Tanhua, T., Hainbucher, D., Schroeder, K., Cardin, V., Álvarez, M., and Civitarese, G.: The Mediterranean Sea system: a review and an introduction to the special issue, Ocean Sci., 9, 789–803, doi:10.5194/os-9-789-2013, 2013b. 1651
Tanhua, T., Waugh, D., and Bullister, J.: Estimating changes in ocean ventilation from the early 1990s CFC-12 and late SF_6 measurements, Geophys. Res. Lett., 40, 927–932, doi:10.1002/grl.50251, 2013c. 1656
Taylor, C. and Roether, W.: A uniform scale to report low-level tritium measurements in water, Int. J. Appl. Radiat. Is., 33, 377–382, 1982. 1656

OSD
10, 1647–1705, 2013

Unterweger, M., Coursey, B., Schima, F., and Mann, W.: Preparation and calibration of the 1987 National Bureau of Standards tritiated-water standards, Int. J. Appl. Radiat. Is., 31, 611–614, 1980. 1656
Vollmer, M. and Weiss, R.: Simultaneous determination of sulfur hexafluoride and three chlorofluorocarbons in water and air, Mar. Chem., 78, 137–148, 2002. 1652
Walker, S. J., Weiss, R. F., and Salameh, P. K.: Reconstructed histories of the annual mean atmospheric mole fractions for the halocarbons CFC-11 CFC-12, CFC-113, and carbon tetrachloride, J. Geophys. Res. Oceans, 105, 14285–14296, doi:10.1029/1999JC900273, 2000. 1653
Warner, M. and Weiss, R.: Solubilities of chlorofluorocarbons 11 and 12 in water and seawater, Deep-Sea Res. Pt. I, 32, 1485–1497, 1985. 1653
Waugh, D., Hall, T., and Haine, T.: Relationships among tracer ages, J. Geophys. Res., 108, C53138, doi:10.1029/2002JC001325, 2003. 1656
Waugh, D., Haine, T. W., and Hall, T. M.: Transport times and anthropogenic carbon in the subpolar North Atlantic Ocean, Deep-Sea Res. Pt. I, 51, 1475–1491, 2004. 1658
Waugh, D., Hall, T., McNeil, B., Key, R., and Matear, R.: Anthropogenic CO_2 in the oceans estimated using transit time distributions, Tellus B, 58, 376–389, 2006. 1658
Waugh, D. W., Vollmer, M. K., Weiss, R. F., Haine, T. W. N., and Hall, T. M.: Transit time distributions in Lake Issyk-Kul, Geophys. Res. Lett., 29, 84-1–84-4, 2002. 1657
Wuest, G.: On the vertical circulation of the Mediterranean Sea, J. Geophys. Res., 66, 3261–3271, 1961. 1649

OSD
10, 1647–1705, 2013

Table 1. Suggested mean ages based on a 2IG-TTD at station 290.

Pressure [dB]	α [%]	Γ_1 [yr]	Γ_2 [yr]	Mean age [yr]
51	0	0	12	12
75	0	0	15	15
202	0	0	25	25
254	0	0	30	30
304	0	0	38	38
404	0	0	46	46
607	0	0	60	60
810	n.a.	n.a.	n.a.	n.a.
1013	n.a.	n.a.	n.a.	n.a.
1267	n.a.	n.a.	n.a.	n.a.
1522	0	0	67	67
1775	0	0	77	77
2031	n.a.	n.a.	n.a.	n.a.
2286	n.a.	n.a.	n.a.	n.a.
2540	n.a.	n.a.	n.a.	n.a.
2600	0	0	60	60

OSD
10, 1647–1705, 2013

Table 2. Suggested mean ages based on a 2IG-TTD at station 305.

Pressure [dB]	α [%]	Γ_1 [yr]	Γ_2 [yr]	Mean age [yr]
26	n.a.	n.a.	n.a.	n.a.
52	n.a.	n.a.	n.a.	n.a.
77	n.a.	n.a.	n.a.	n.a.
102	10	59	1	7
152	40	23	1	10
203	50	28	1	15
254	60	33	2	20
304	50	63	2	33
405	60	81	2	50
506	70	125	2	88
608	70	207	7	147
1013	80	320	8	258
1522	80	246	5	197
2032	70	279	4	196
2543	90	138	7	125
3053	80	167	6	134
4087	90	101	4	91

OSD
10, 1647–1705, 2013

Table 3. Suggested mean ages based on a 2IG-TTD at station 317.

Pressure [dB]	α [%]	Γ_1 [yr]	Γ_2 [yr]	Mean age [yr]
51	n.a.	n.a.	n.a.	n.a.
102	n.a.	n.a.	n.a.	n.a.
203	n.a.	n.a.	n.a.	n.a.
304	n.a.	n.a.	n.a.	n.a.
405	n.a.	n.a.	n.a.	n.a.
507	n.a.	n.a.	n.a.	n.a.
811	n.a.	n.a.	n.a.	n.a.
1014	n.a.	n.a.	n.a.	n.a.
1267	70	757	3	531
1776	80	370	6	297
2032	90	230	18	208
2542	90	246	4	221
3268	n.a.	n.a.	n.a.	n.a.

OSD
10, 1647–1705, 2013

Table 4. Suggested mean ages based on a 2IG-TTD at station 323.

Pressure [dB]	α [%]	Γ_1 [yr]	Γ_2 [yr]	Mean age [yr]
52	n.a.	n.a.	n.a.	n.a.
103	n.a.	n.a.	n.a.	n.a.
203	50	127	2	64
304	60	135	2	82
406	70	170	3	120
812	80	228	8	184
1523	80	222	4	178
2031	60	411	4	248
2287	60	332	1	200
2542	60	294	3	177
2798	60	364	2	219

OSD
10, 1647–1705, 2013

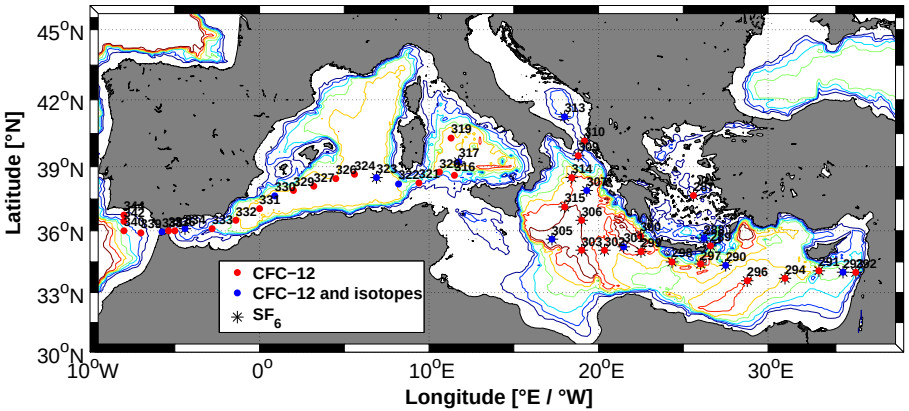

Fig. 1. Transient tracer sample stations of the M84/3 cruise from Istanbul to Vigo. Red dots indicate CFC-12 only stations, blue dots CFC-12 as well as tritium and black stars SF_6 stations.

OSD
10, 1647–1705, 2013

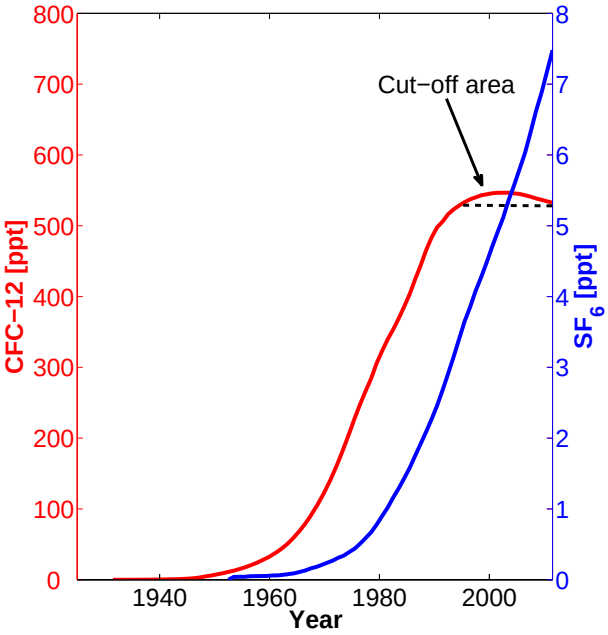

Fig. 2. Atmospheric histories of CFC-12 in red and of SF_6 in blue. The decreasing trend of CFC-12 produces a cut-off area between 1994–2011, i.e. any CFC-12 concentration above 532 ppt provides only inconclusive information about ventilation.

OSD
10, 1647–1705, 2013

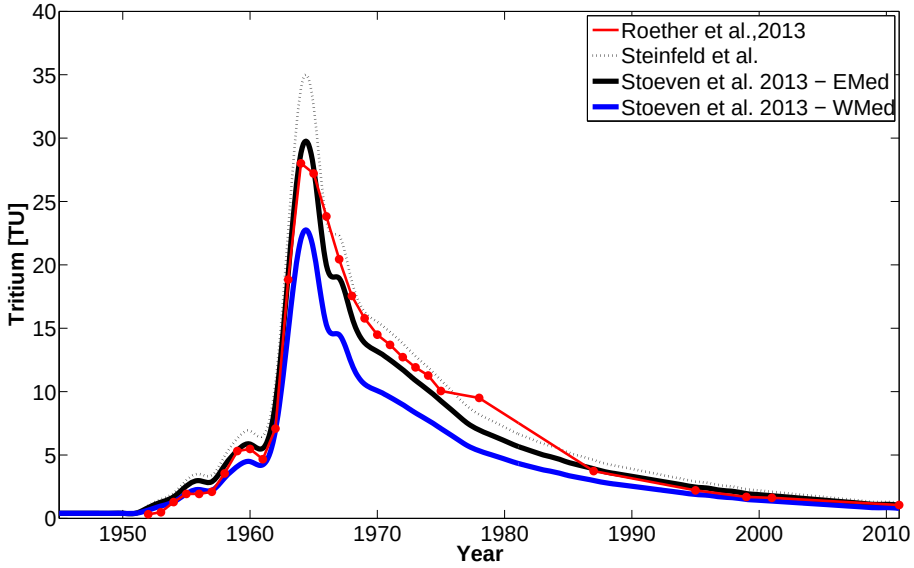

Fig. 3. Input functions of tritium. The dotted black curve shows the decay based input function of the Mediterranean Sea by R. Steinfeld. The black and blue curves describe the off set corrected input functions for the eastern and western Mediterranean Sea. The red curve shows the suggested input function by Roether et al. (2013) of the eastern Mediterranean Sea.

OSD
10, 1647–1705, 2013

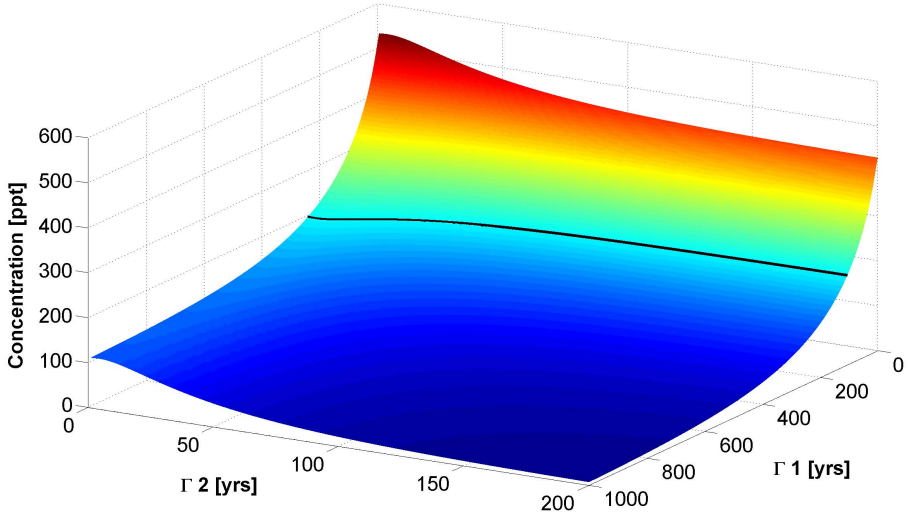

Fig. 4. Example mean age matrix of CFC-12. The color-coding denotes the concentration of CFC-12 (in ppt, also on the Z-axis) with a black concentration contour line at 200 ppt; X and Y axis denotes the mean age of the 2IG distributions that make up the TTD. The combination of all three dimensional tracer matrices provides the needed information to constrain a 2IG-TTD, see text.

OSD
10, 1647–1705, 2013

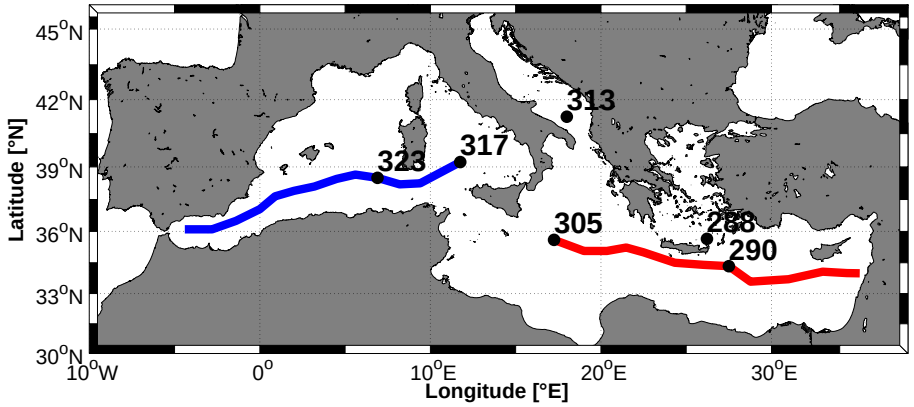

Fig. 5. Sections and key stations of the transient tracer analysis. The red line shows the EMed section, the blue line the WMed section and the black dots the key stations.

OSD
10, 1647–1705, 2013

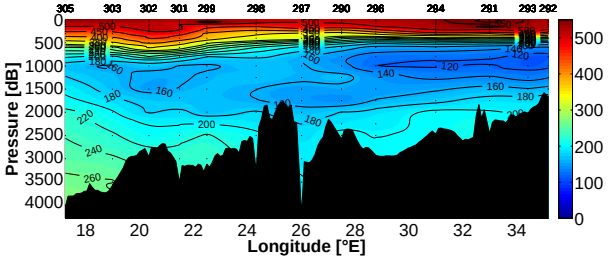

(a)

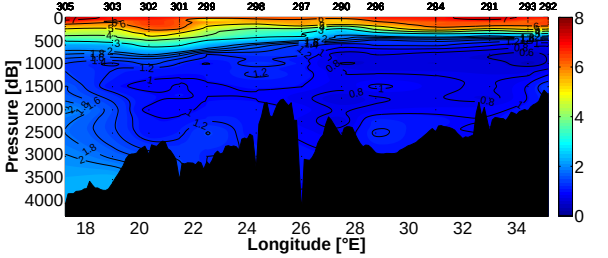

(b)

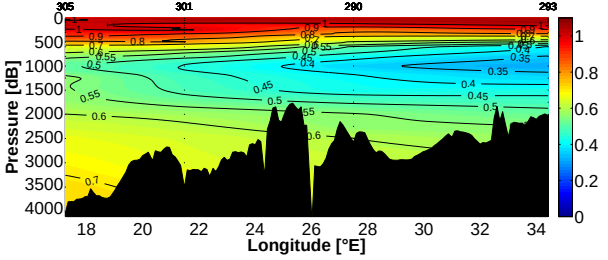

(c)

Fig. 6. Transient tracer concentrations in the EMed during April 2011 (cruise M84/3), red line in Fig. 5. **(a)** CFC-12 in ppt **(b)** SF_6 in ppt **(c)** tritium in TU.

OSD
10, 1647–1705, 2013

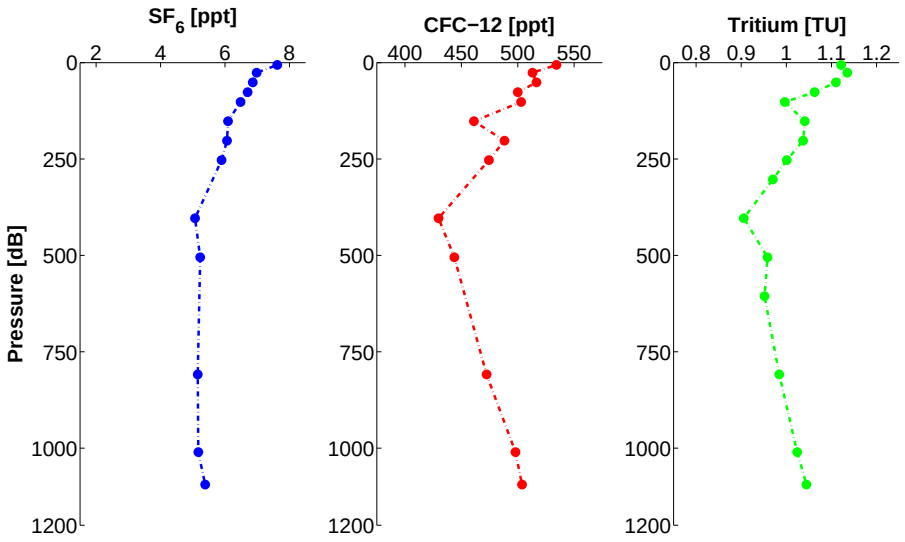

Fig. 7. Profiles of transient tracers in the Adriatic Sea at station 313 during April 2011. All three transient tracer show high concentrations throughout the whole water column.

OSD
10, 1647–1705, 2013

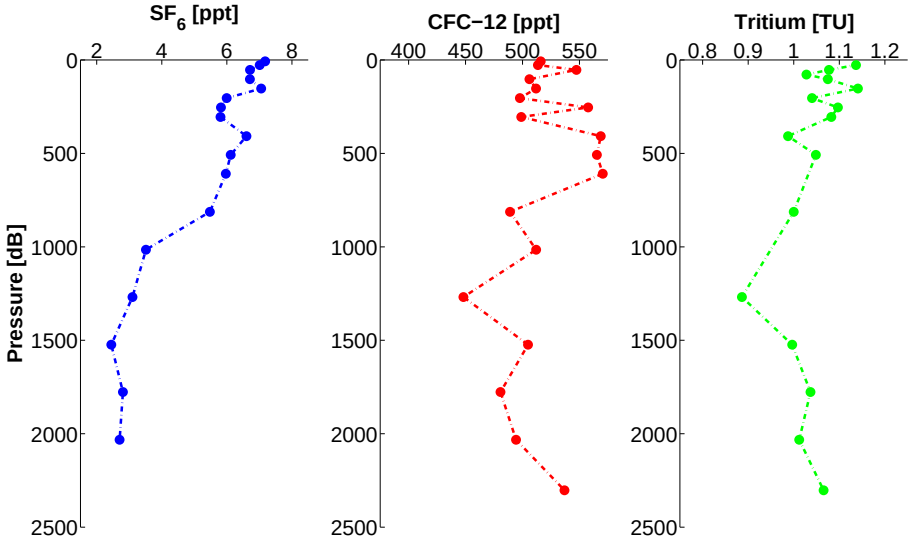

Fig. 8. Profiles of transient tracers in the Cretan Sea at station 288 during April 2011. SF_6 shows a clear concentration gradient whereas the CFC-12 and tritium concentrations scatter around their maximum values.

OSD
10, 1647–1705, 2013

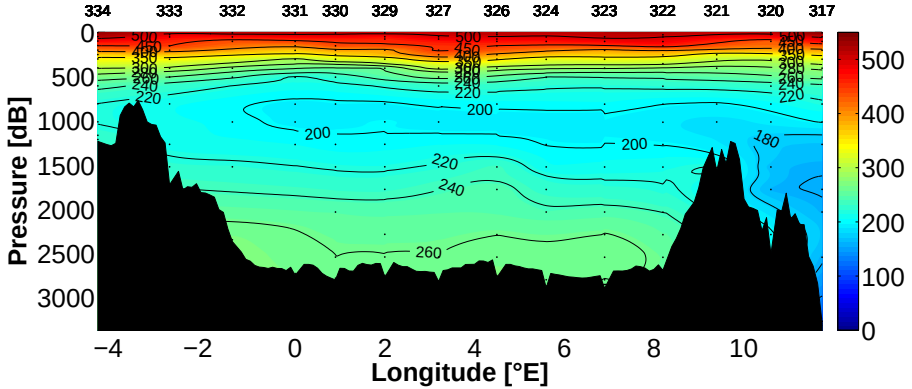

Fig. 9. CFC-12 concentration in ppt of the western Basin and the Tyrrhenian Sea, blue line in Fig. 5.

OSD
10, 1647–1705, 2013

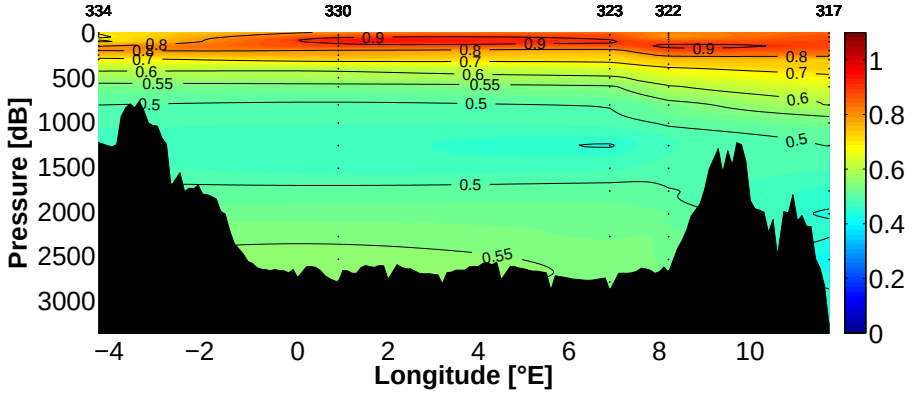

Fig. 10. Tritium concentration in TU of the western Basin and the Tyrrhenian Sea, blue line in Fig. 5.

OSD
10, 1647–1705, 2013

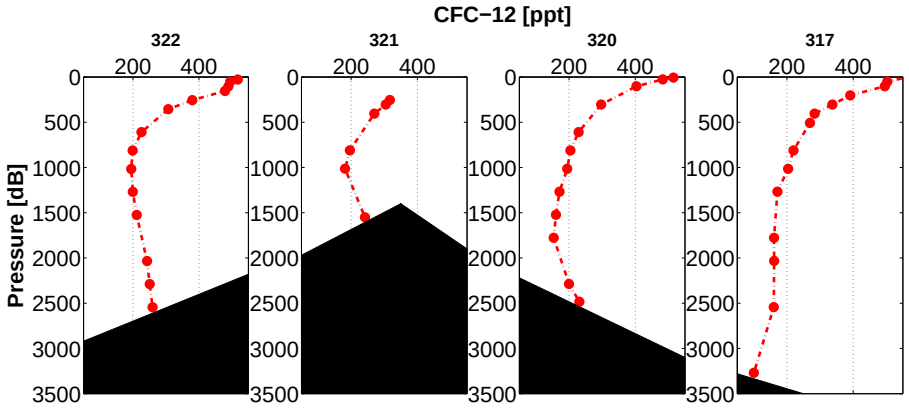

Fig. 11. CFC-12 concentration in ppt along the shallow sill between Sardinia and Sicily. The elevated CFC-12 concentration of the bottom layer indicates the overflow of WMDW into the Tyrrhenian Sea. The depth of each station is indicated by the black patch in each panel.

OSD
10, 1647–1705, 2013

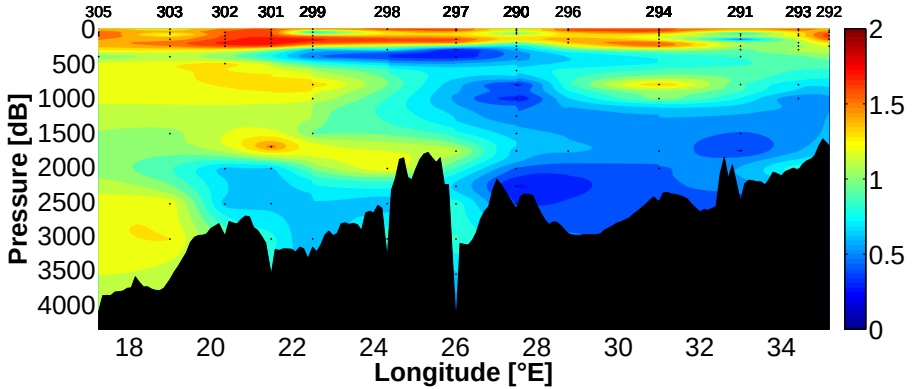

Fig. 12. Determined $^{\Delta}/_{\Gamma}$ ratios in the EMed based on the transient tracer couple CFC-12 and SF_6. The black points indicate the constrained data points of the section.

OSD
10, 1647–1705, 2013

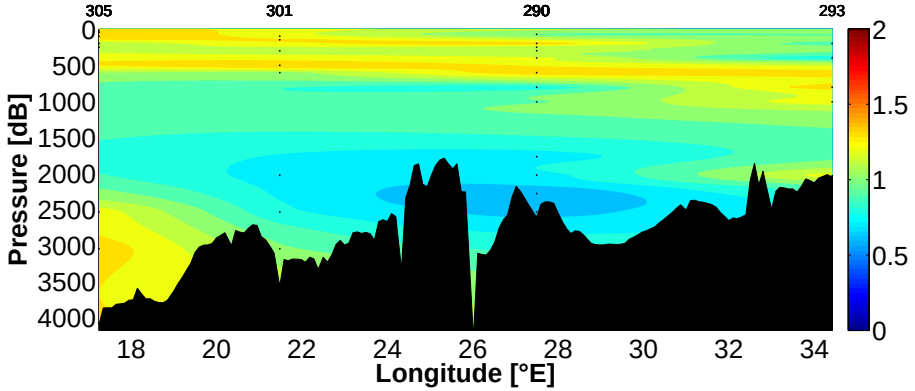

Fig. 13. Determined $^{\Delta}/_{\Gamma}$ ratios in the EMed based on the transient tracer couple tritium and SF_6 and the corrected tritium input function. The black points indicate the constrained data points of the section.

OSD
10, 1647–1705, 2013

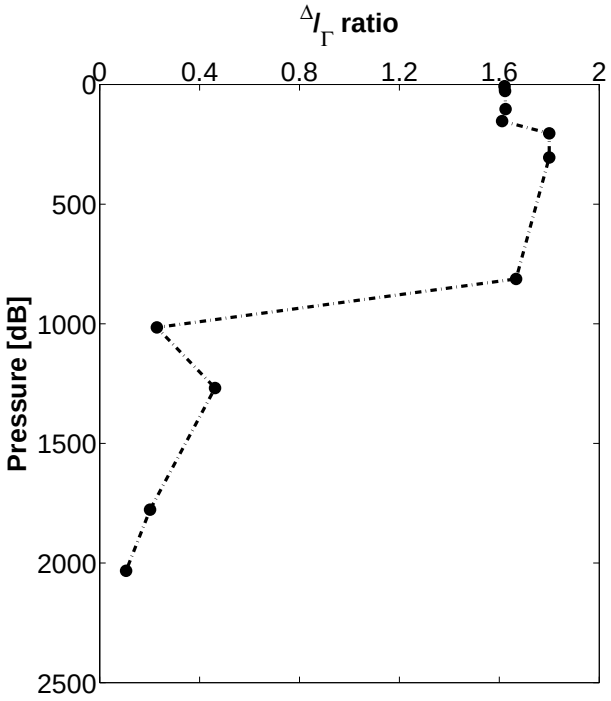

Fig. 14. Determined $^{\Delta}/_{\Gamma}$ ratios in the Cretan Sea obtained by the transient tracer couple CFC-12 and SF_6.

OSD
10, 1647–1705, 2013

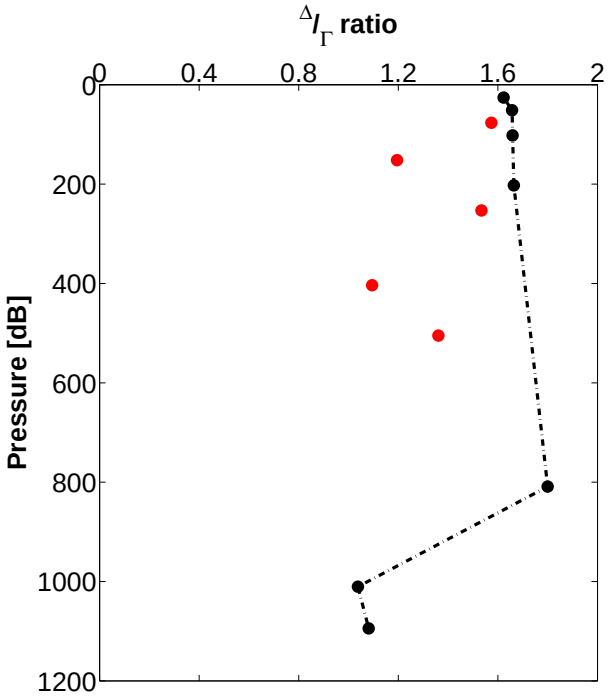

Fig. 15. Determined $^{\Delta}/_{\Gamma}$ ratios in the Adriatic Sea obtained by the transient tracer couple CFC-12 and SF_6. The red dots indicate ratios with a mean age difference > 5 yr and thus defined as non-constrained within the 1IG-TTD model.

OSD
10, 1647–1705, 2013

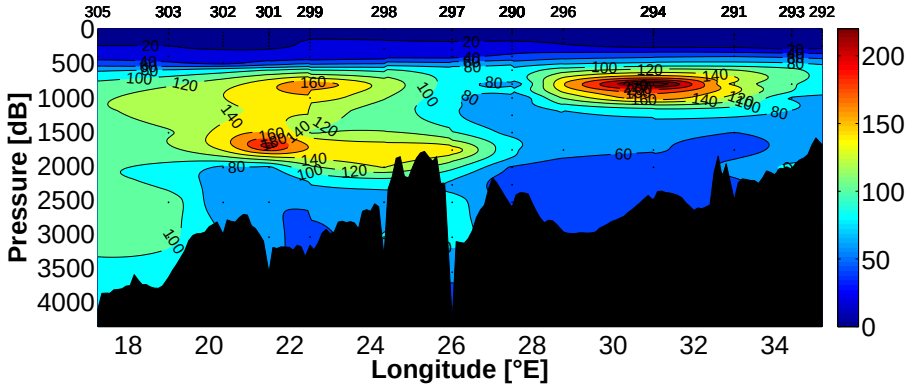

Fig. 16. Mean ages of the EMed based on an 1IG-TTD constrained by the transient tracer couple CFC-12 and SF_6.

OSD
10, 1647–1705, 2013

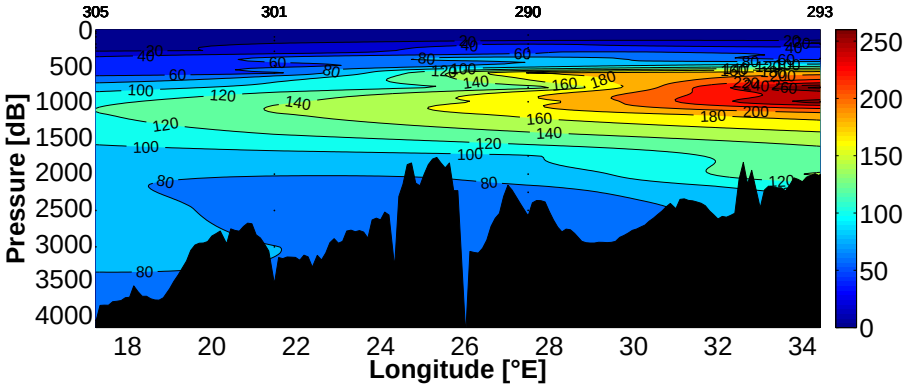

Fig. 17. Mean ages of the EMed based on an 1IG-TTD constrained by the transient tracer couple tritium and SF_6 and the corrected tritium input function.

OSD
10, 1647–1705, 2013

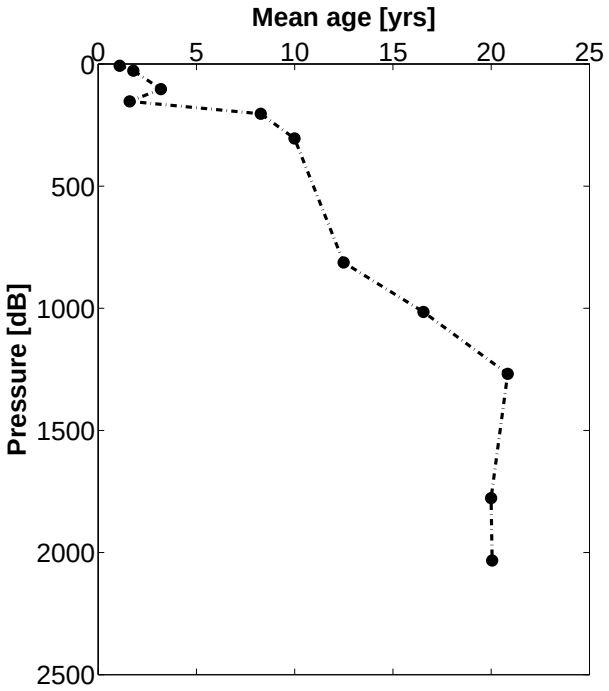

Fig. 18. Determined mean ages in the Cretan Sea based on SF_6 and an 1IG-TTD constrained by the transient tracer couple CFC-12 and SF_6.

OSD
10, 1647–1705, 2013

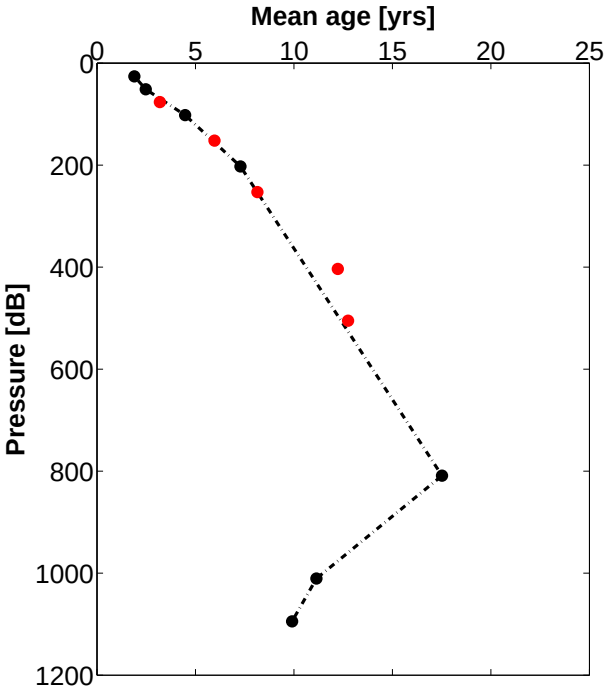

Fig. 19. Determined mean ages in the Adriatic Sea based on SF_6 and an 1IG-TTD constrained by the transient tracer couple CFC-12 and SF_6. The red dots show mean ages based on approached constraints with a mean age difference of more than 5 yr compared to the CFC-12 mean ages.

OSD
10, 1647–1705, 2013

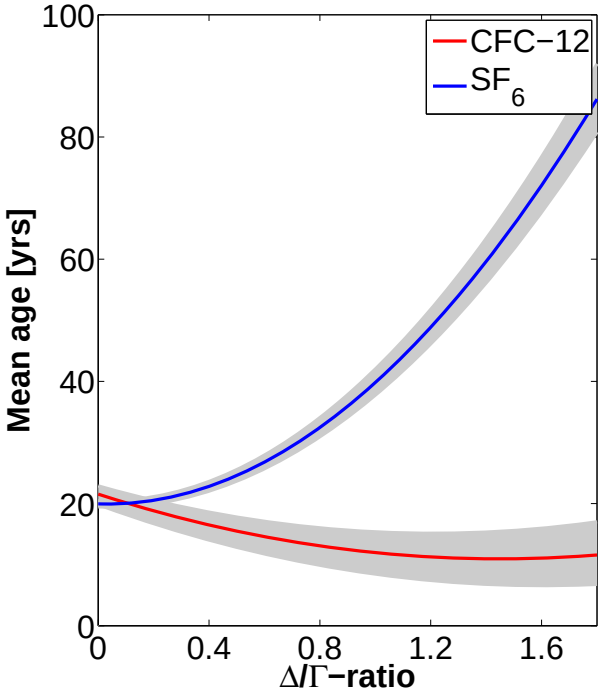

Fig. 20. Mean age functions of CFC-12 and SF_6 at station 288 in the Cretan Sea at 2030 m depth with an error range of 4 % analytical error.

OSD
10, 1647–1705, 2013

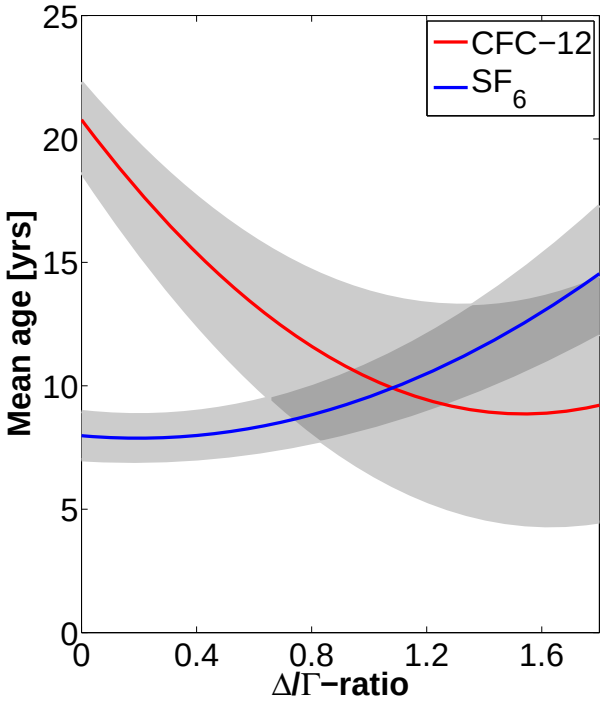

Fig. 21. Mean age functions of CFC-12 and SF_6 at station 313 in the Adriatic Sea at 1094 m depth with an error range of 4 % analytical error.

OSD
10, 1647–1705, 2013

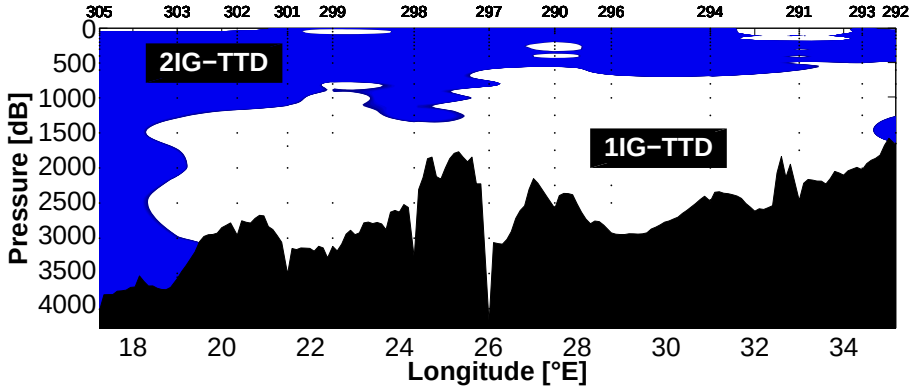

Fig. 22. Differences of tracer ages between CFC-12 and SF_6. The white shading describes tracer age differences below and the blue shading above 10 yr.

OSD
10, 1647–1705, 2013

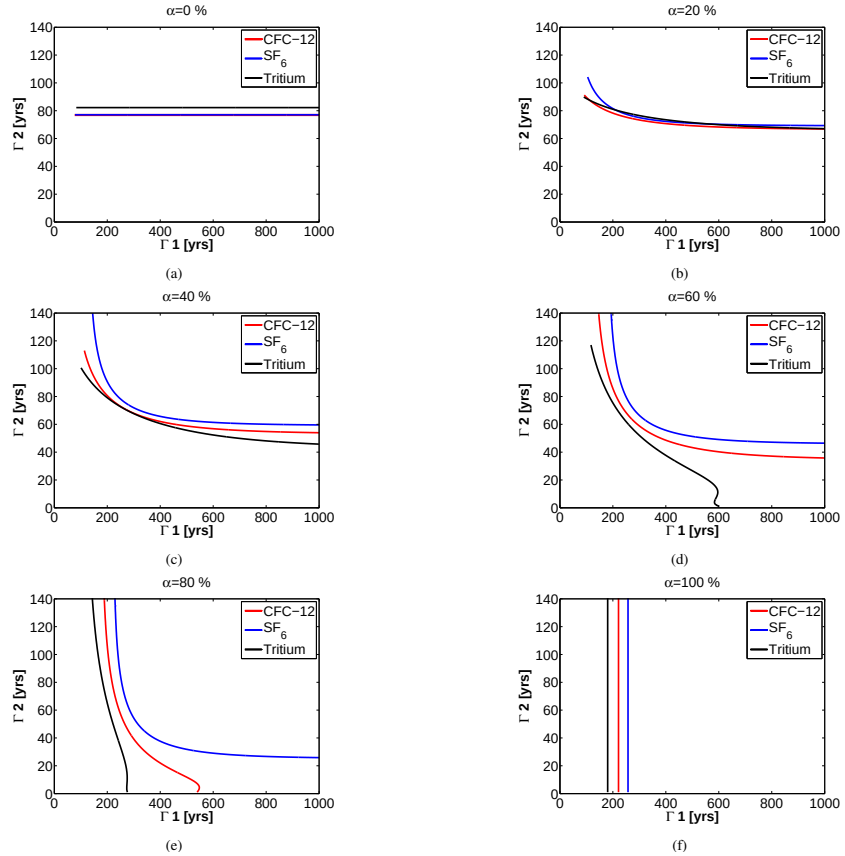

Fig. 23. Example of a mean age calculation from three transient tracers (CFC-12, SF_6 and tritium) at station 290 at 1775 m depth. The six panels are for different fractions of the older water mass (α value). The Δ/Γ ratios are set to 0.6 for the younger water mass, and to 1.4 for the older water mass. Panel **(a)** shows the selected result, see text.

OSD
10, 1647–1705, 2013

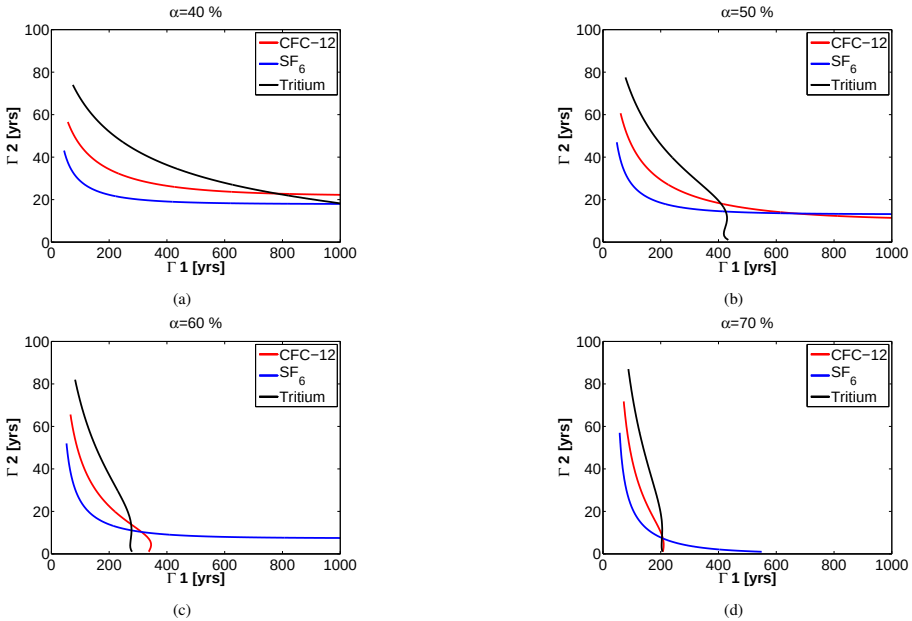

Fig. 24. Example for a mean age calculation from three transient tracers (CFC-12, SF_6 and tritium) at station 305 at 608 m depth. Panel **(d)** shows a triple intersection of all three transient tracer concentrations and thus a solution for the mean age at this data point of 147 yr.

OSD
10, 1647–1705, 2013

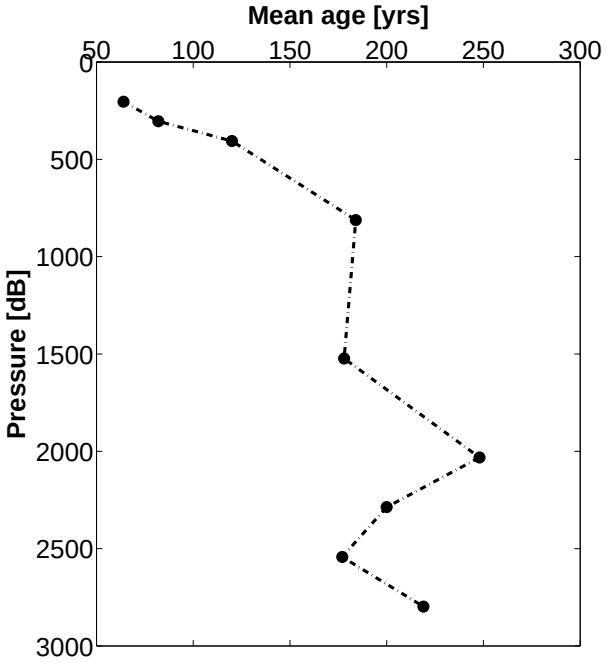

Fig. 25. Mean ages at station 323 in the WMed based on an 2IG-TTD constrained by the transient tracer couple CFC-12 and SF_6.

OSD
10, 1647–1705, 2013

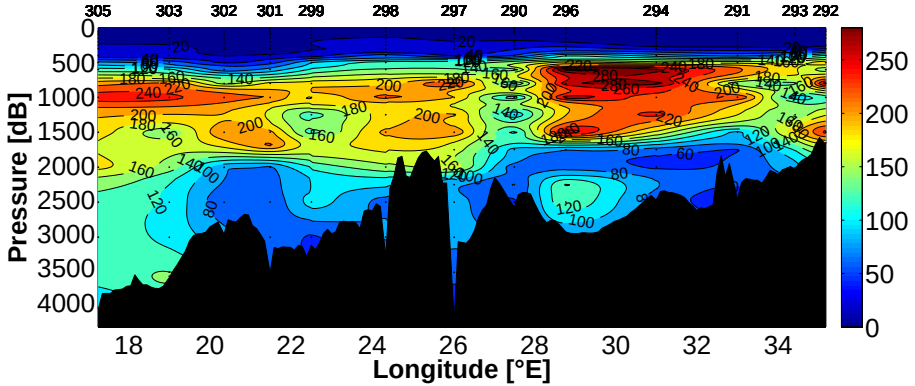

Fig. 26. Best estimate of mean ages of the EMed based on the combination of an 1IG-TTD and a predefined 2IG-TTD constrained by the transient tracer couple CFC-12 and SF_6.

OSD
10, 1647–1705, 2013